Polymer Testing 131 (2024) 108322

Contents lists available at ScienceDirect

Polymer Testing

journal homepage: www.elsevier.com/locate/polytest

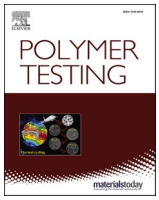

Crystallization of poly(lactic acid) nucleated with the sorbitol TBPMN

F.F.G. Sebek [a], O.J. Nguon [b], A. Bartos [b], M. ten Brinke [b], M. van Drongelen [c], H. Gojzewski [a], J. Lefas [b,d], G.J. Vancso [a,b,*]

[a] Materials Science and Technology of Polymers & Sustainable Polymer Chemistry, MESA+ Institute for Nanotechnology, University of Twente, 7500AE, Enschede, the Netherlands
[b] Sulis Polymers B.V., Theo van Loonstraat 21, 7552GN, Hengelo, the Netherlands
[c] Production Technology Group, Faculty of Engineering Technology, University of Twente, 7500AE, Enschede, the Netherlands
[d] Ingenia Polymers International S.A., 21-25 Allée Scheffer, 6th Floor, Luxembourg L-2520, Luxembourg

ARTICLE INFO

Keywords:
Poly(lactic acid)
Crystallinity
Nucleating agents
Atomic force microscopy

ABSTRACT

We report on the crystallization of poly(lactic acid) (PLA) films in the presence of a sorbitol-based nucleating agent; 1,2,3-tridesoxy-4,6:5,7-bis-O-[(4-propylphenyl) methylene]-nonitol (TBPMN). Dispersion of the nucleating agent was performed by solution-mixing and melt-blending. Crystallization behavior was studied by differential scanning calorimetry (DSC). The structure and morphology were characterized by wide-angle X-ray scattering (WAXS), optical imaging, and atomic force microscopy (AFM). A significant impact of the nucleating agent was observed at or above a threshold concentration of 2 wt%, which was assigned to the solubility limit of TBPMN. The degree of crystallinity reached up to 39.6 % with 2 wt% TBPMN. An influence of the dispersion method was observed on the peak temperature of crystallization (T_{cp}). While T_{cp} decreased slightly for solution-mixed films, a sigmoidal trend was noted for melt-blended samples. Under isothermal conditions at 100 °C, the crystallization half-time was lowered from 6.5 min to 1.0 min. Avrami analysis pointed to the formation of 2-dimensional or 3-dimensional crystalline domains; WAXS data revealed α- and α'-crystals, depending on the dispersing method. AFM imaging showed a nanosized fibrillar network of the nucleator within the PLA matrix, demonstrating that TBPMN acted as a soluble self-assembly nucleator.

1. Introduction

Growing concerns about the environmental, economic, and health impact of fossil-based polymers have driven intensive research on the design, materials chemistry, and technology of biodegradable substitutes. Poly(lactic acid) (PLA) represents one of the most promising bio-based and biodegradable alternatives, owing to its high strength, good processability, compostability, and economic attractiveness [1,2]. However, significant limitations persist, and the development of a broader range of applications remains hindered by its slow crystallization rate and low degree of crystallinity [3], fast physical ageing [4], sensitivity to hydrolysis [5], and poor thermal stability. Additionally, PLA is a chiral polyester, and different morphologies can be observed for its two enantiomers [6]. Thus, greater control over the crystallization behavior of PLA would result in significant improvements over its mechanical, thermal, and barrier performance and enable broader utilization.

The crystallization of PLA can be tuned by promoting a high nucleation density and short nucleation induction period, which can be achieved by using nucleating agents [7–10]. A wide range of such agents has been investigated for PLA, including inorganic, organic, and macromolecular compounds. Talc displayed a high nucleation efficiency in PLA and is often used as a reference compound [11,12]. Silica, carbon nanotubes, and graphene oxide are other examples of inorganic materials acting as nucleating agents [13–15]. However, low solubility and particle aggregation often impinge on their nucleation efficiency and material properties. On the other hand, organic compounds can display a high affinity and miscibility with the polymer matrix. Natural organic materials such as natural rubber (NR) can also be used to increase the crystallinity of PLA. NR, however, should usually be applied in larger amounts, and it has a negative effect on the ultimate tensile properties of PLA [16–18]. A particular class of organic compounds – known variously as clarifiers, low molar-mass organogelators, supramolecular, or (partially) soluble self-assembly nucleators (SSANs) – were shown to

* Corresponding author. Materials Science and Technology of Polymers & Sustainable Polymer Chemistry, MESA+ Institute for Nanotechnology, University of Twente, 7500AE, Enschede, the Netherlands.
E-mail address: g.j.vancso@utwente.nl (G.J. Vancso).

https://doi.org/10.1016/j.polymertesting.2023.108322
Received 23 October 2023; Received in revised form 13 December 2023; Accepted 30 December 2023
Available online 31 December 2023

exhibit a high nucleation efficiency for PLA and other thermoplastics [19]. As opposed to traditional nucleators, SSANs dissolve in the polymer melt during a heating cycle and self-assemble upon cooling into 2- or 3-dimensional structures, such as needles [7], dendritic structures [20], or fibrillar networks [21]. These heterogeneous structures promote a high nucleation density and rapid crystallization. Although a complete understanding of the mechanism at play remains elusive, evidence suggests that designer SSANs are well-dispersed in the PLA melt as well as promote strong intermolecular interactions and conformational regulations of the PLA chains during cooling [19]. Such soft templating method has been demonstrated effective using arylamides [7,22,23], aliphatic amides [24], hydrazides [25,26], aliphatic acids [27], and sorbitol compounds [28–31]. Sorbitol-based nucleators are of particular interest as SSANs, having been historically employed as performant clarifying agents in polypropylene (PP) [29]. Lai et al. demonstrated that the first generation of sorbitol clarifiers, *viz*. 1,3:2,4-dibenzylidene-D-sorbitol (DBS) was also applicable in PLA, self-assembled into fibrils in the polymer melt, and increased the nucleation rate of PLA [31]. Petchwattana et al. later reported an increased degree of crystallinity in PLA using the third-generation sorbitol-type nucleator, dimethylbenzylidene sorbitol (DMDBS), while maintaining good clarity [28].

As the next step toward a better understanding and control of PLA crystallization, we report here our investigation on the role of the fourth-generation sorbitol-based nucleator, *viz*. 1,2,3-tridesoxy-4,6:5,7-bis-O-[(4-propylphenyl) methylene]-nonitol (TBPMN). This compound is the most recent sorbitol-type nucleator marketed. It exhibits superior performance in PP compared to previous generations, displaying greater solubility, lower processing temperatures, reduced yellowing, better organoleptics, and greater optical transparency [30,32]. In the present study, TBPMN was dispersed in the polymer matrix by employing solvent-mixing or melt-blending techniques. The concentration investigated ranged from 1 wt% to 5 wt%. The peak temperature of melt crystallization (T_{cp}), melting temperature (T_m), degree of crystallinity (X_c), crystallization half-time ($t_{1/2}$), as well as the crystalline structure within neat PLA and the PLA/sorbitol materials were determined using differential scanning calorimetry (DSC), thermogravimetric analysis (TGA), polarised-light optical microscopy (PLOM), wide-angle X-ray scattering (WAXS), and atomic force microscopy (AFM).

2. Experimental section

2.1. Materials

PLA Ingeo 4032D (1.4–2.0 % D-isomer content) was obtained from NatureWorks LLC. (Minnetonka, MN, USA). It has an apparent M_w determined by SEC in chloroform (PS calibration) of 202.7 kg/mol and $Đ = 2.0$, a density of 1.24 g/cm^3, while its melt flow rate (MFR) is 3.9 g/10 min at 190 °C and 2.16 kg load. The PLA pellets and 1,2,3-tridesoxy-4,6:5,7-bis-O-[(4-propylphenyl) methylene]-nonitol (TBPMN, Milliken, Millad® NX® 8000) were dried in a vacuum oven at 60 °C overnight prior to use. Dichloromethane (DCM, Sigma Aldrich, anhydrous, ≥99.8 %) was used as received.

2.2. Sample preparation

The nucleator was dispersed in the polymer matrix by either solvent-mixing or melt-blending, at a concentration ranging from 1 wt% to 5 wt %.

Solution-cast films. Solvent-mixing was performed by dissolving 0.5 g of PLA in DCM (20 mL). The desired amount of nucleator was mixed with 2 mL of DCM in a separate vial and stirred for 45 min. The nucleator solution was then added dropwise to the polymer solution under vigorous stirring, and mixing was continued for 30 min. Solution-cast films were obtained by depositing the solutions in an ethanol-washed glass Petri dish, dried under ambient conditions in a fume hood for 2 h, and then transferred to a vacuum oven at 90 °C overnight.

Melt-blended and compression molded films. Melt-blending was conducted in a HAAKE PolyLab QC (Thermo Fisher Scientific Inc., Waltham, MA, US) modular torque rheometer, equipped with a HAAKE Rheomix 600 QC internal mixer and roller-type rotors R600 (chamber volume with rotors: 69 cm^3). The mixer was heated to 180 °C, and mixing was performed at 50 rpm. PLA pellets (60 g) were added to the mixer, which was closed with an automatic feeding ram and melted for 1 min. The ram was lifted, and the nucleator powder was added to the chamber within 1 min, after which the chamber was closed, and mixing continued for another 5 min. The melt-blended samples were compression molded using a Fontijne hot press (Fontijne Holland BV, Vlaardingen, The Netherlands). A mold (0.2 mm in thickness) was placed between two metal plates covered with PTFE sheets and was filled with the samples. The plates were preheated in the press at 180 °C for 3 min. The force was then increased to 100 kN and maintained for 2 min. The temperature was then lowered with water cooling below T_g (circa 50 °C).

2.3. Analysis

The DSC measurements were carried out with a Pyris 1 (PerkinElmer Inc. Waltham, MA, US) and a DSC 250 (TA Instruments Inc., New Castle, DE, US) equipment. The temperature profile was the following: heating from 20 °C to 220 °C at 5 °C/min, holding at 220 °C for 5 min, and cooling to 20 °C at 5 °C/min. Two successive cycles were executed. Measurements were performed in triplicates. For isothermal measurements, the sample was heated from 20 °C to 200 °C (5 °C/min), holding at 200 °C for 5 min, rapidly cooled to 100 °C (320 °C/min), and maintained at this temperature for 40 min. The degree of crystallinity was calculated as $X_c = \Delta H_x/(\Delta H_{f0}[1\text{-}f]) \times 100$, where ΔH_x is the enthalpy of crystallization from the melt, ΔH_{f0} is the heat of fusion (taken as 93 J/g for a fully crystalline PLA [33]), and f the mass fraction of the nucleator.

A TGA 550 (TA Instruments Inc., New Castle, DE, US) device with an autosampler was used for the TGA measurements. N_2 atmosphere was established by purging with N_2 gas at 40–60 mL/min. For each measurement, ca. 5 mg of sample was used. The specimens were placed in a Pt pan and maintained at 30 °C for 1 min. Heating was performed at 10 °C/min up to 500 °C. When the measurement was completed, the temperature was returned to 30 °C.

The polymer crystallization was monitored using an Olympus BX60 optical microscope (Olympus Co., Tokyo, Japan) in transmission mode. The temperature was controlled with a hot stage, increasing from 30 °C to 200 °C at 5 °C/min.

A Discover D8 (Bruker Co. Billerica, MA, US) instrument was used for WAXS measurements in transmission mode, using a 2D detector. The X-ray source was Cu (Kα), the voltage was 40 kV, and the current 40 mA. The slit width was set to 0.6 mm. The reflection spectra were obtained at 2θ, ranging from 10° to 30°. A pre-thermal treatment was carried out with the hot stage under the same conditions used for PLOM imaging.

AFM measurements were conducted on the melt-blended 2 wt% PLA/TBPMN film sample using a Veeco NanoScope 4 MultiMode 8 instrument, equipped with an HC GV scanner, non-contact/tapping mode cantilever, and a peristaltic pump with water/ice for scanner cooling. Image analysis was done using the Nanoscope Analysis 1.8 software. The sample was first scanned at 20 °C, then heated and scanned at 100 °C. The sample was then melted to 175 °C, cooled to 100 °C for analysis, and further down to 24 °C for another scanning in tapping mode.

3. Results and discussions

3.1. Neat PLA and TBPMN

The thermal properties of the neat PLA were determined by non-isothermal DSC under quiescent conditions after erasing the thermal history are shown in Fig. S1. The polymer thermal behavior was characteristic for this semi-crystalline material and displayed a T_g of 58 °C and a cold crystallization peak in the range of 100–150 °C. The polymer

melted with a sharp peak at 167 °C (T_m) but displayed only a small melt crystallization peak (X_c = 1.9 %) around 101 °C upon cooling at 5 °C/min, indicating its poor crystallization behavior.

TBPMN (Fig. 1a), used as a sorbitol-type nucleator, was provided as a white powder with no discernible features (Fig. 1b). After dissolution in dichloromethane, the molecules self-assembled into short fibrils, about 50 μm in length and less than 10 μm in diameter (Fig. 1c). The thermal behavior of TBPMN alone, measured by DSC, revealed that there was no exothermic peak occurring when processed below its melting temperature. However, when heated above its melting point at 247.2 °C, a sharp exothermic peak was measured upon cooling at 230 °C (Fig. S2).

3.2. PLA/TBPMN solution-cast films

The thermal behavior of the PLA/TBPMN films was studied by DSC, and the thermograms for all the samples are reported in Fig. S3. The T_g values (Table 1) of all nucleated samples remained comparable to that of the neat resin, indicating little influence of the nucleator on chain mobility upon heating.

The nucleator, however, exhibited a significant influence on the melt crystallization behavior of PLA. The corresponding DSC thermograms of the solution-cast samples are displayed in Fig. 2a–b. At a low nucleator concentration (≤1 wt%), only a small and broad exothermic peak was observed at an onset crystallization temperature below 100 °C, indicative of the poor crystallization behavior of PLA. At or above a threshold nucleator concentration of 2 wt%, a prominent exothermic peak indicated a rapid melt crystallization of PLA around 110 °C. Noteworthy, a second small exothermic peak appeared at more elevated temperatures when the nucleator concentration was above 2 wt%. It was particularly pronounced in the sample with 4 wt% TBPMN, occurring at 149 °C. All the nucleated samples with ≥2 wt% TBPMN exhibited no cold crystallization peak (see Fig. 2b and **S3**) when subjected to a subsequent heating cycle, as opposed to PLA samples with a lower nucleator content, indicating efficient melt crystallization of the former samples.

The change in T_{cp} as a function of the nucleator concentration is commonly used to assess the efficiency of a nucleator [8,24,31,34,35]. It can be correlated to the spherulite size, lamellae thickness, and optical properties. As shown in Fig. 2c, T_{cp} exhibited a sigmoidal increase with TBPMN concentration, characteristic of the influence of SSANs on crystallization kinetics [34,36]. At low TBPMN concentration (1 wt%), T_{cp} remained low (96.1 ± 0.5 °C); however, a sharp increase was observed as the concentration of TBPMN reached 2 wt%, with a T_{cp} of 107.4 ± 4.6 °C. The rapid increase in nucleation efficiency with concentration has been linked to the solubility of the nucleator in the polymer melt [34]. For TBPMN, the solubility limit in PLA may therefore be estimated to be ca. 2 wt%. T_{cp} remained approximately 110 °C as the nucleator concentration was increased to 3 wt% and 5 wt%. Unexpectedly, a drop in T_{cp} occurred at 4 wt% TBPMN. This composition also correlated with the appearance of a second exothermic event (Fig. 2a) and is further discussed below.

A similar sigmoidal trend was observed between the degree of crystallinity and TBPMN content in PLA (Fig. 2d). An effect of the nucleator was observed when at least 2 wt% of TBPMN was added, reaching an average X_c of 39.5 ± 2.1 %. A similar X_c (see Table 1) was also obtained after a second heating cycle. Noteworthy, a double melting peak was observed at or above the threshold concentration of 2 wt% during the second heating cycle (Fig. 2b and S3). Such double peaks have been attributed variously to melt-recrystallization of α and α' (also referred to as δ) crystals [37], dual lamellae populations, or dual crystal structures [38]. However, in spite of the previous data on T_{cp}, a drop in X_c was not observed with 4 wt% of TBPMN.

The reflection spectra from WAXS analysis of the solution-cast films, processed with the same thermal treatment as used for DSC analysis, are reported in Fig. S4 (with assigned 2θ peak positions). While neat PLA remained amorphous, PLA with TBPMN exhibited the presence of α-crystals (1 wt%, 2 wt%, and 4 wt% TBPMN). The sample with 3 wt% TBPMN uniquely exhibited a reflection peak at 22.2°, indicating the presence of α-crystals but also reflections shifted to lower angles (by

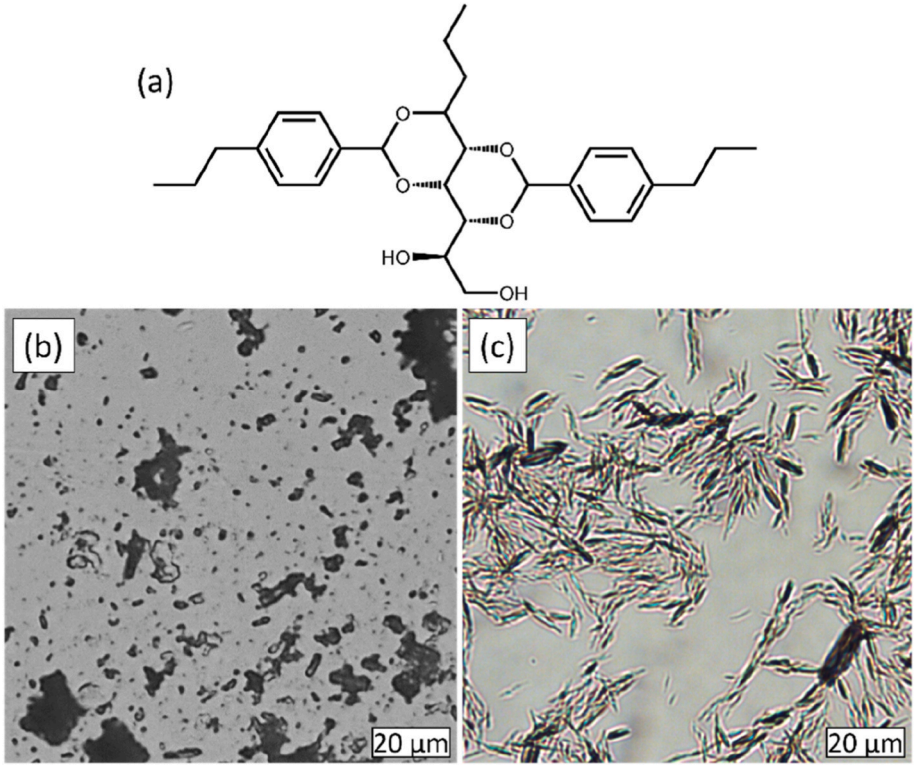

Fig. 1. The chemical structure of the nucleator used in the experiments (a), as well as optical micrographs of the TBPMN powder (b) and after dissolution in dichloromethane (c). The scale bars represent 20 μm.

Table 1
Characteristic values determined by DSC: glass transition temperature (Tg); crystallization temperature (Tc), enthalpy of crystallization (Hc); cold crystallization temperature (Tcc); enthalpy of cold crystallization (Hcc); melt temperature (Tc); heat of fusion (Hm); degree of crystallization (Xc).

	TBPMN (wt.%)	Tg [°C][a]			Tc [°C][b]			Hc [J/g][b]			Tcc [°C][c]			Hcc [J/g][c]			Tm [°C][c]			Hm [J/g][c]			Xc_1 [%][d]			Xc_2 [%][e]		
Solution mixing	0	61,9	±	0,0	97,8	±	1,3	−2,6	±	0,6	121,5	±	5,8	−29,4	±	0,1	167,3	±	1,9	36,2	±	2,0	2,7	±	0,6	7,3	±	2,0
	1	58,4	±	1,8	96,1	±	0,5	−8,5	±	2,5	96,3	±	4,3	−22,2	±	8,0	167,8	±	0,8	37,6	±	1,8	9,3	±	2,7	16,4	±	10,0
	2	59,2	±	2,2	107,4	±	4,6	−36,0	±	1,9							168,7	±	0,2	39,9	±	1,9	39,5	±	2,1	42,0	±	2,0
	3	60,8	±	0,7	111,3	±	1,7	−37,8	±	3,5							168,7	±	0,3	39,2	±	2,2	41,9	±	3,8	40,9	±	2,2
	4	59,0	±	4,0	104,4	±	1,8	−39,2	±	4,0							168,2	±	0,6	39,4	±	3,3	43,9	±	4,5	40,7	±	3,4
	5	58,5	±	3,1	109,6	±	4,1	−35,3	±	2,4							168,7	±	0,6	38,2	±	0,9	39,9	±	2,8	39,0	±	0,9
Melt blending	0	57,3	±	0,7	116,1	±	0,8	−7,6	±	1,1	103,8	±	1,6	−23,7	±	3,2	169,1	±	0,5	37,0	±	1,9	8,2	±	1,2	14,3	±	5,4
	1	56,7	±	1,0	114,9	±	1,6	−9,7	±	3,1	99,2	±	3,1	−23,0	±	7,4	169,0	±	1,9	40,2	±	2,7	10,6	±	3,4	24,1	±	5,6
	2	56,6	±	0,9	109,0	±	12,5	−29,6	±	8,1	93,6	±	3,1	−8,7	±	10,5	167,8	±	0,9	39,4	±	0,1	32,5	±	8,9	40,8	±	0,9
	3	56,4	±	0,3	109,6	±	0,5	−39,7	±	1,3							169,5	±	1,7	41,2	±	1,2	44,0	±	1,5	43,0	±	1,2
	4	56,9	±	1,5	102,6	±	2,3	−37,8	±	3,1							167,9	±	0,4	40,9	±	0,8	42,4	±	3,4	42,2	±	0,8
	5	58,0	±	0,4	101,8	±	0,4	−39,7	±	4,3							167,8	±	0,0	39,7	±	0,0	44,9	±	4,9	40,6	±	0,0

[a] Determined from the first heating curve.
[b] Determined from the cooling curve.
[c] Determined from the second heating curve.
[d] Calculated from the cooling curve.
[e] Calculated from the second heating curve.

about 0.2°) for the characteristic peaks at 16.7° and 19.1°, also revealing the presence of α′-crystals [39,40]. This is in agreement with the DSC thermographs for this sample, which showed a small exothermic peak prior to the melting peak upon heating, indicating an α′ to α transition [41], and also a double melting peak, possibly assigned to the melting of α- and α′-crystals at different temperatures. However, some contradictions have also been observed in the DSC thermogram and WAXS pattern of 1 wt% TBPMN concentration sample, which suggest some extent of heterogeneity in the samples. The average crystallite size was comparable for all the crystalline samples, ca. 32.2 nm, suggesting little influence of the nucleator on the crystal size.

The morphology during crystallization was monitored by PLOM (Fig. 3), exposing the materials to the same thermal treatment used during the DSC measurements. Crystallization upon cooling could be clearly visualized for all the samples, with an onset crystallization temperature increasing with nucleator concentration. When using 1 wt % TBPMN, spherulite formation occurred at 108 °C, while with 5 wt% TBPMN, the onset crystallization temperature was increased to 130 °C. The spherulite size was the smallest with 2 wt% TBPMN, with an average diameter of 3.33 ± 0.8 μm. Notably, the spherulites grew larger with decreasing and increasing TBPMN concentration, reaching 18.79 ± 2.6 μm at 1 wt% and 10.3 ± 2.6 μm at 5 wt%, respectively.

From the PLOM images, we can infer that at a low concentration (1 wt%) fibrous network did not form. The absence of this fibrous network may be attributed to the nucleating agent concentration not reaching the critical threshold required for self-assembly. Only a few heterogeneous nucleation sites were present, resulting in a low nucleation density and the formation of large spherulites. By increasing the nucleator concentration to 2 wt% (i.e., above its solubility limit), a homogeneous distribution of TBPMN resulted in the self-assembly of a fibrillar network. The dense network with a small mesh size promoted the nucleation of a higher number of spherulites, which remained small due to their impinged growth. At a higher nucleator concentration (3–5 wt%), aggregation of TBPMN particles resulted in a network with thicker fibrils and a larger mesh size. Such a network exhibited a lower nucleation density and resulted in the crystallization of larger spherulites.

3.3. Melt-blended samples

3.3.1. Non-isothermal crystallization

The nucleation efficiency of SSANs largely depends on their thermal history and processing conditions [34]. From the practical point of view, the significance of melt processing is much greater than film/solution casting; thus, an extensive investigation was performed on such samples. Industrially, nucleators are usually added in a powder form to polymer pellets and processed by melt extrusion.

To study the influence of the sample preparation method, melt-blended samples of PLA and TBPMN were prepared using an internal mixer. TGA measurements (see Fig. S5) proved no significant mass loss at the chosen processing temperature (180 °C) in the mixing chamber. The overall DSC thermograms of the melt-blended samples are displayed in Fig. S6. The traces from the cooling and second heating cycle are reported in Fig. 4a–b. As noted for the solution-cast samples, at a low nucleator concentration (≤1 wt%), only a small and broad exothermic peak was observed at an onset crystallization temperature of around 120 °C, indicative of the poor crystallization behavior of PLA. Above the threshold concentration, with 2 wt% nucleator, two peaks were visible. A prominent crystallization peak occurred at 103 ± 3.5 °C, indicating a greater crystallization rate in the presence of TBPMN.

As shown in Fig. 4c, the T_{cp} of melt-blended samples was found to decrease slightly with increasing nucleator concentration (from 116.1 ± 0.8 °C to 101.8 ± 0.4 °C, with 0 wt% and 5 wt% TBPMN, respectively). The deviation in the crystallization behavior of the sample prepared with 2 wt% TBPMN must be noted here. The test of this sample was repeated multiple times, and a similar behavior was detected in all cases which supports our earlier assumption about the threshold

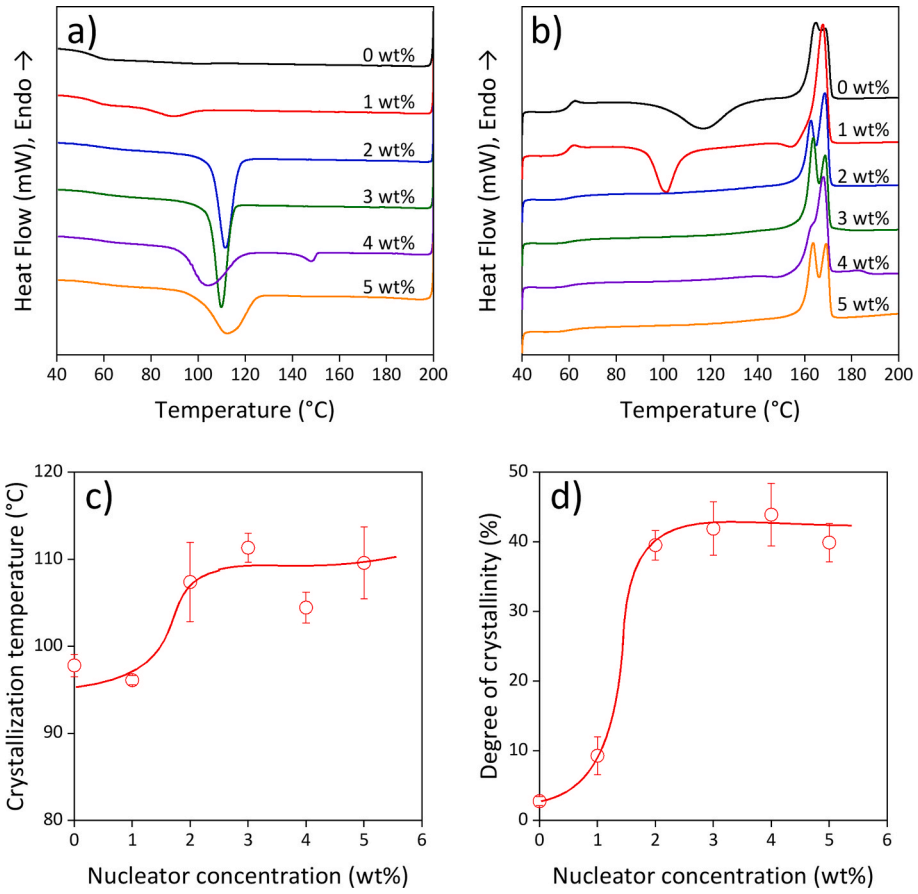

Fig. 2. DSC thermograms, upon cooling from the melt (a) second heating cycle (b), of solution-cast samples; corresponding to neat PLA (0 wt%) and PLA samples mixed with TBPMN. Traces have been shifted for visibility. A significant shift can be observed at or above 2 wt% nucleator concentration in the peak temperature of crystallization (c) and degree of crystallinity (d). The latter was calculated from the cooling curve. Lines are added as guides to the eye.

concentration of the nucleator. Also, the trend notably deviates from the sigmoid trend observed with the solution-cast samples (Fig. 2c). The higher T_{cp} and X_c of the melt-blended samples compared to those of the solution-cast films at low nucleator concentrations ($\leq$1 wt%) may be ascribed to polymer degradation during processing. Melt-blending of PLA has been shown to induce thermal degradation and chain scission. The decrease in molar mass and correlated increase in chain mobility result in an enhanced nucleation rate upon cooling [42]. We note that a higher T_{cp} may be particularly advantageous during processing, allowing shorter cycle times. The degree of crystallinity in melt-blended samples displayed a similar sigmoidal trend as for solution-cast samples when the TBPMN concentration was increased (Fig. 4d). A sharp increase in X_c is reported at or above 2 wt% TBPMN, reaching a plateau at around $X_c = 40$ %.

Interestingly, at higher nucleator concentrations ($\geq$2 wt%), T_{cp} remained lower or comparable to that of the solution-cast samples, with the notable occurrence of a second exothermic event. As discussed above, this event was also associated with a reduction in the T_{cp} of the solution-cast sample prepared with 4 wt% of TBPMN. Noteworthy, the peak temperature and enthalpy change of this second exothermic event increased with nucleator concentration, ranging from 121.5 °C to 151.9 °C and 0.29 J/g to 2.6 J/g from 2 wt% to 5 wt% TBPMN, respectively (Fig. 5). The exothermic event reported at high temperatures is reminiscent of the thermal behavior in mixtures of enantiomeric PLAs. In such systems, a crystallization peak at high temperatures is well-reported and ascribed to stereocomplex formation in the melt, acting as efficient nucleating sites during cooling [43,44]. A correlation between concentration and crystallization temperature has been reported in such compositions, which exhibit a network structure spawned by stereocomplex crystals [45,46]. In comparison, PLA/TBPMN mixtures may exhibit a comparable network assembly and the formation of supramolecular structures, acting as efficient nucleating sites. Such interactions appear particularly favored when adding 4 wt% TBPMN, either when processed from the solution or in the melt. Further investigation would be required to determine the supramolecular interactions that may be taking place between the TBPMN molecules and PLA chains.

Furthermore, the influence of the nucleator concentration on T_{cp} may be quantitatively correlated to the spherulite size and optical properties. Horváth et al. proposed that the sorbitol nucleator network promotes small-sized spherulites and helps improve clarity in PP [35]. In PLA/TBPMN samples, the nucleator above its threshold concentration (*viz.* 2 wt%) promotes a higher T_{cp} which may be advantageous in terms of optical properties.

The melt-blended PLA/TBPMN materials were compression molded to thin films and subjected to the same thermal treatment employed for the non-isothermal DSC analysis. The films were then analyzed by WAXS. The spectra are shown in Fig. S7. In all cases, the 2θ reflections indicated the formation of α′-crystals (which peaks were shifted to lower angles by about 0.2° relative to the characteristic peaks of the α-form crystals, reported at 16.7° (200/110) and 19.1° (203) [40,47]. No other reflection peaks were observed for the neat PLA and 1 wt% TBPMN samples, so only α′-crystals formed. For PLA samples with a TBPMN content $\geq$2 wt%, characteristic peaks of α-crystals were also detected at 14.7° (010) and 22.2° (015). Moreover, the even-numbered (00X) reflections were absent, indicating that both α- and α′-crystals structures were present [48]. The mixed crystalline structure was also apparent by DSC exhibiting double melting peaks in a subsequent heating cycle. The crystallite size was comparable in all the crystalline samples and

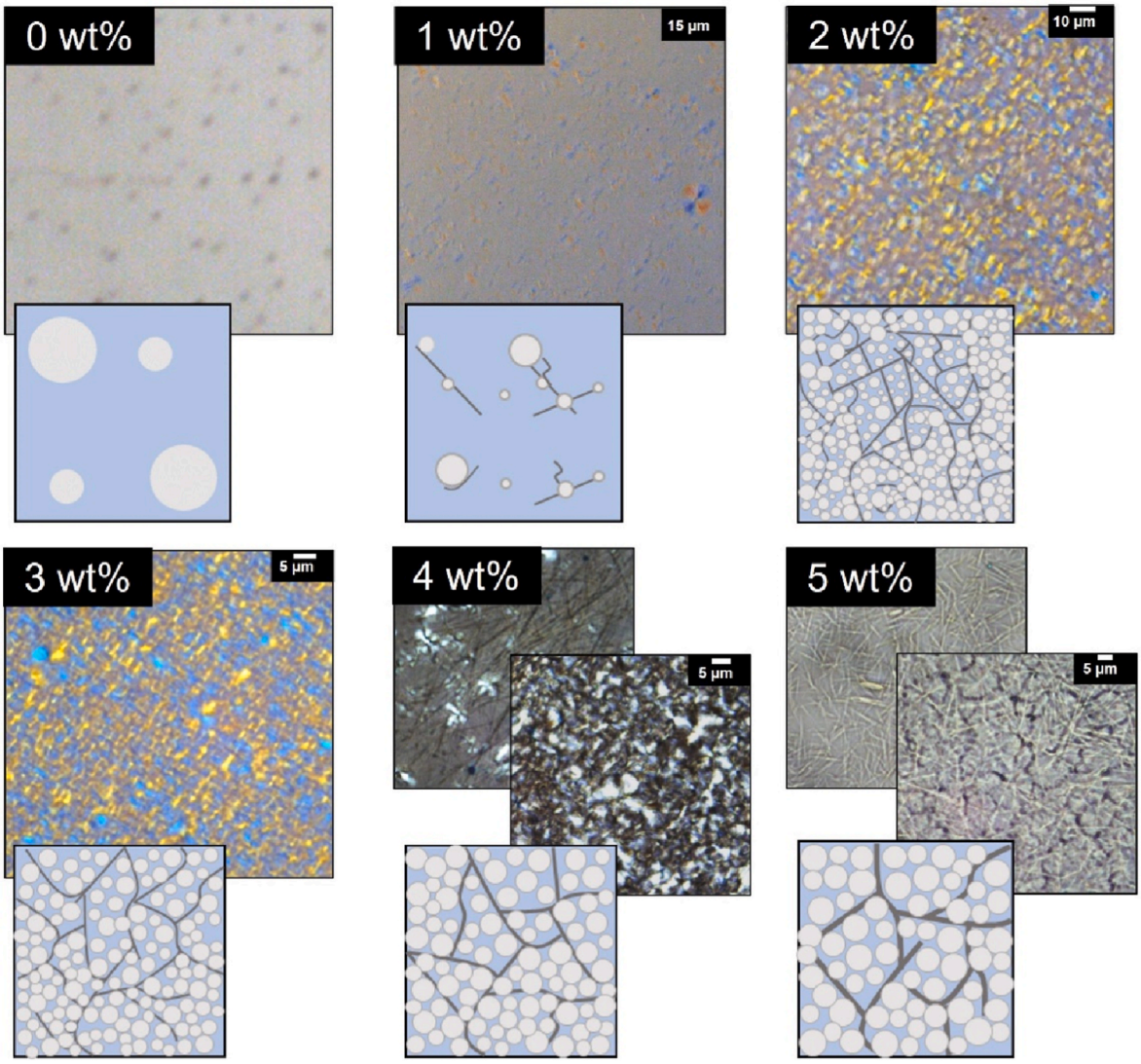

Fig. 3. PLOM images (top) of solvent-mixed PLA/TBPMN samples (TBPMN concentration ranging from 0 wt% to 5 wt%) after cooling from the melt. Proposed schematic representations (bottom) of the fibrillar network and spherulite formation.

calculated to be 29.3 nm, slightly smaller than for solution-cast samples. It can be concluded that TBPMN promoted the crystallization of PLA, and the formation of α-crystals, although a distorted α′ crystalline structure also formed during the melt processing.

3.3.2. *Isothermal crystallization*

The isothermal crystallization behavior of the PLA/TBPMN melt-blended samples at 100 °C is illustrated in Fig. S8. The corresponding kinetics of the change in the relative degree of crystallinity for different nucleator concentrations are represented in Fig. 6a. Neat PLA displayed the lowest crystallization rate, exhibiting a crystallization half-time ($t_{1/2}$) of 6.5 min. Using 1 wt% TBPMN, $t_{1/2}$ was decreased to 5.4 min; and was the lowest when adding 2 wt% TBPMN ($t_{1/2}$ = 1.0 min). Further addition of TBPMN (3–5 wt%) slightly increased $t_{1/2}$; however, that change is insignificant. As noted for T_{cp} and X_c, a threshold crystallization behavior occurred at or above 2 wt% TBPMN content, exhibiting a sharp increase in the crystallization kinetics. This rate compares favorably to other sorbitol/PLA systems (DBS, DMBS), with a reported $t_{1/2}$ ca. 5 min [28,31].

The isothermal crystallization behavior was further analyzed by applying the Avrami model [49]. All the experimental data showed a good fit to the theory in the primary crystallization range (Fig. 6b). The calculated values of the Avrami exponent *n* at different TBPMN content are reported in Table 2. For all the samples, except for 4 wt% PLA/TBPMN, *n* ranged between 2.4 and 3.1, which compares well to reported values for neat PLA [50]. Values of *n* approaching 3 suggest a transition from a two-dimensional to a three-dimensional athermal growth of spherulites promoted by TBPMN [51]. The sample with 4 wt% TBPMN exhibited the highest *n* value of 3.3, hinting at a transition to a more sporadic three-dimensional growth [52], which may be induced by particular supramolecular complexes formed at this composition.

3.3.3. *AFM analysis*

The self-assembly of sorbitol-type nucleators into a fibrillar network is highly dependent on the processing conditions, thermal history, and concentration. Although several techniques have been used to investigate the fibrillation process, it has remained a challenge to monitor in-situ the network formation from the polymer melt [53]. As shown in Fig. 3 for the solution-cast samples, fibrils formation was monitored by optical microscopy but only at high nucleator concentrations (≥4 wt%) and for micron-sized fibrils. However, it is expected that rather nano-sized fibrils provide the most efficient nucleation and clarification performance [34].

In this study, we employed AFM to help visualize the nucleator

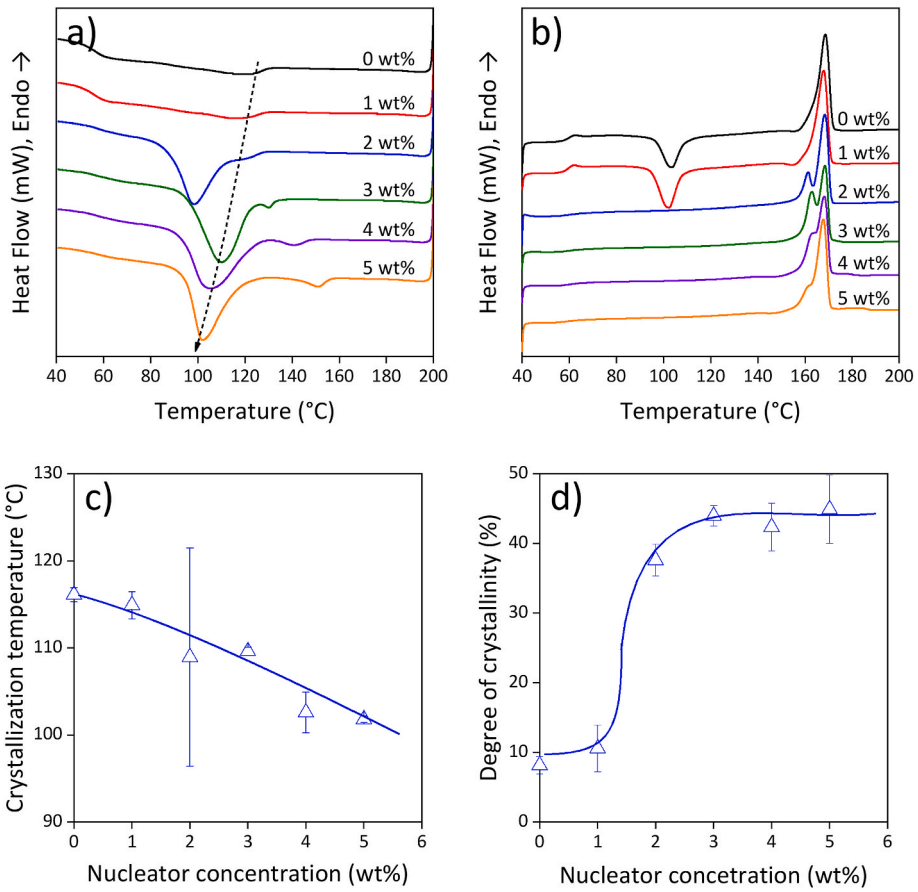

Fig. 4. DSC thermograms, upon cooling from the melt (a) second heating cycle (b), of melt-blended; corresponding to neat PLA (0 wt%) and PLA samples mixed with TBPMN. Traces have been shifted for visibility. A decrease can be observed in the peak temperature of crystallization with increasing nucleator concentration (c) and a significant shift in the degree of crystallinity at or above 2 wt% of TBPMN (d). The latter was calculated from the cooling curve. Lines are added as guides to the eye.

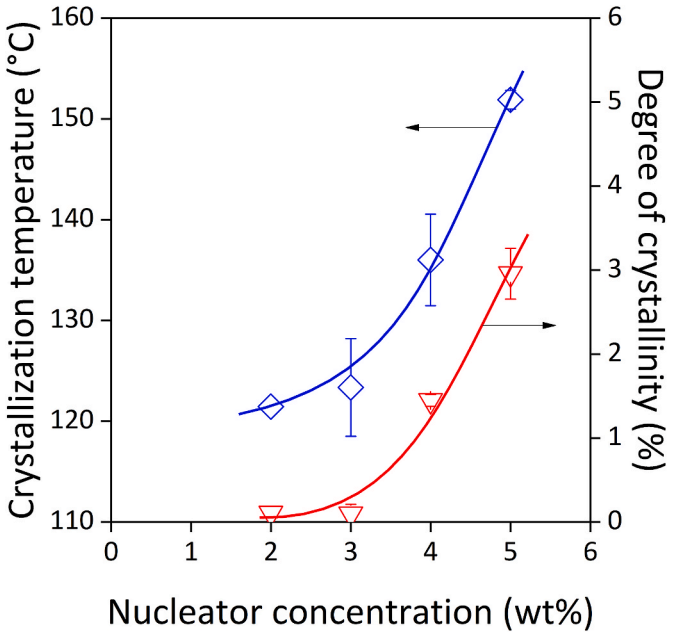

Fig. 5. Crystallization temperature and degree of crystallinity of the second (small) exothermic event occurring during cooling from the melt of PLA/TBPMN melt-blended samples.

network formation in the polymer melt of a melt-blended sample containing 2 wt% TBPMN. As shown in Fig. 7a, the sample displayed a smooth surface with only a few fibrils visible at 20 °C. Upon heating to 100 °C, the softer PLA matrix allowed the resolution of a dense network of fibrils visible at the sample surface and displayed an average diameter of 0.03 ± 0.01 μm. The fibrils, which made up the network, exhibited a twisted helical structure, as shown in the magnified image in Fig. 7c and d. It has been reported that polarity and solvent effects influence the self-assembly of sorbitol compounds and can promote the formation of helical structures [54]. The sample was then melted at 175 °C and cooled down to 100 °C. As shown in Fig. 7d, further growth of the fibrils took place during this thermal process and exhibited an average diameter of 0.18 ± 0.09 μm at 100 °C. Fibrils were also still visible at the surface by cooling the sample to room temperature and had an average diameter of 0.17 ± 0.06 μm at 24 °C (Fig. 7e).

4. Conclusions

The crystallization behavior of PLA was studied in the presence of the sorbitol-based nucleating agent TBPMN. Dispersion of the nucleator in the polymer matrix was obtained by employing two different methods: solution mixing and melt-blending. TBPMN self-assembled in short fibrils in dichloromethane prior to addition to PLA. On the other hand, TBPMN was added as a powder to melted PLA and self-assembled upon exposure to higher processing temperatures. The concentration of the nucleator significantly influenced the crystallization behavior. At or above a threshold concentration of 2 wt% TBPMN, a noticeable increase in the degree of crystallinity of PLA was measured by DSC, reaching approximately 40 %. This threshold concentration was associated with

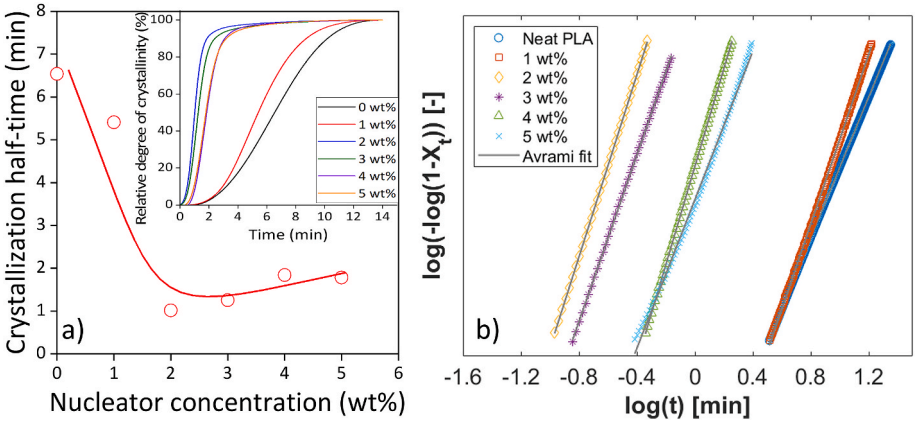

Fig. 6. Isothermal crystallization at 100 °C of melt-blended PLA/TBPMN samples, measured by DSC. (a) The crystallization half-time as a function of TBPMN, and (b) plots based on the Avrami model. Inset, the corresponding relative degree of crystallinity over time.

Table 2
Values of the Avrami exponent (n) and its two constituting factors (n_d, dimension, and n_n time-dependence) for different TBPMN content, obtained from the analysis of melt-blended samples.

Concentration	n	n_d	n_n
Neat PLA	2.44	2	0.44
1 wt%	2.87	2	0.87
2 wt%	3.08	3	0.08
3 wt%	2.82	2	0.82
4 wt%	3.31	3	0.31
5 wt%	2.49	2	0.49

the solubility limit of TBPMN in PLA. A dependence on the processing method was found for the peak temperature of crystallization upon cooling, which was used to evaluate the nucleation performance. While T_{cp} of the melt-blended samples decreased slightly with TBPMN concentration, it exhibited a sigmoidal correlation in solution-cast samples, with a marked increase at or above 2 wt% TBPMN. A prominent exothermic event was observed at 4 wt% TBPMN, attributed to the formation of superstructures between the PLA chains and TBPMN. The peak temperature of this event was found to increase with the nucleator concentration. The crystallization half-time of the PLA/TBPMN samples was measured by isothermal crystallization at 100 °C by DSC and was found to be the lowest at 2 wt% TBPMN, decreasing from 6.5 min for neat PLA to 1.0 min. From WAXS measurements, the crystalline structures were found to be dependent on the processing method. Solution-mixed samples were primarily composed of α-crystals, while melt-blended samples displayed a mixture of α- and distorted α′-crystals. The nucleator concentration did not influence the crystallite size. Avrami analysis revealed crystallization proceeding generally by the

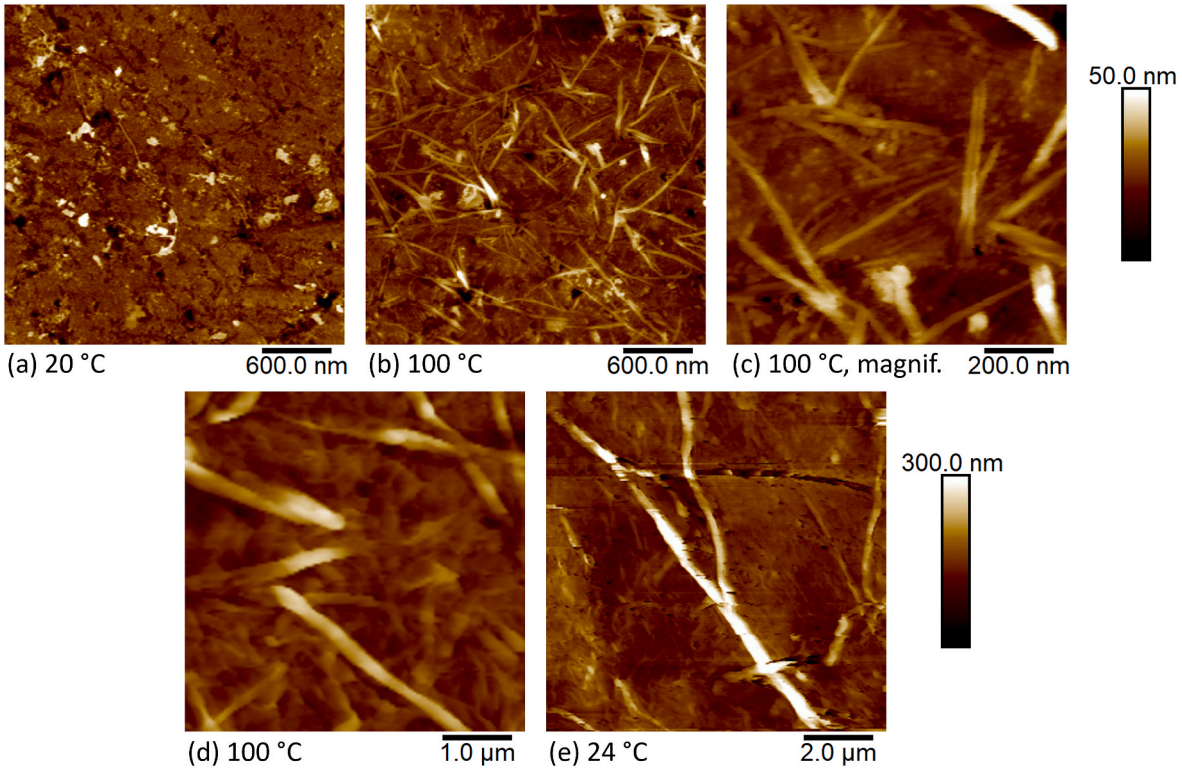

Fig. 7. AFM height images (scan size: 3 µm) of the melt-blended PLA/TBPMN (2 wt%) film sample measured at (a) 20 °C, after heating to (b) 100 °C; and after thermal treatment at 175 °C and cooling to (d) 100 °C, and further cooling to (e) 24 °C. Image (c) is a magnification of image (b), acquired with a scan size of 1 µm.

three-dimensional athermal growth of spherulites, while with 4 wt% TBPMN, a more pronounced sporadic crystal growth was observed. AFM imaging revealed the formation of nanosized fibrils at the surface of melt-blended film samples. Upon heating, the size of the fibrils increased from 0.03 ± 0.01 μm to 0.18 ± 0.09 μm. Soluble self-assembly nucleators are performant additives used to improve the crystallinity and clarity of commodity plastics and have shown promise in PLA materials. Further research in the structure and supramolecular interactions with PLA chains may spawn a new range of applications for this type of nucleator.

CRediT authorship contribution statement

F.F.G. Sebek: Data curation, Investigation. **O.J. Nguon:** Data curation, Investigation, Methodology, Writing – original draft, Writing – review & editing. **A. Bartos:** Data curation, Investigation, Visualization, Writing – original draft, Writing – review & editing. **M. ten Brinke:** Data curation, Investigation. **M. van Drongelen:** Data curation, Investigation. **H. Gojzewski:** Data curation, Investigation. **J. Lefas:** Conceptualization. **G.J. Vancso:** Conceptualization, Methodology, Supervision, Writing – original draft, Writing – review & editing.

Declaration of competing interest

The authors declare that they have no known competing financial interests or personal relationships that could have appeared to influence the work reported in this paper.

Data availability

The data that has been used is confidential.

Appendix A. Supplementary data

Supplementary data to this article can be found online at https://doi.org/10.1016/j.polymertesting.2023.108322.

References

[1] S. Farah, D.G. Anderson, R. Langer, Physical and mechanical properties of PLA, and their functions in widespread applications — a comprehensive review, Adv. Drug Deliv. Rev. 107 (2016) 367–392, https://doi.org/10.1016/j.addr.2016.06.012.

[2] L.T. Lim, R. Auras, M. Rubino, Processing technologies for poly(lactic acid), Prog. Polym. Sci. 33 (2008) 820–852, https://doi.org/10.1016/j.progpolymsci.2008.05.004.

[3] S. Saeidlou, M.A. Huneault, H. Li, C.B. Park, Poly(lactic acid) crystallization, Prog. Polym. Sci. 37 (2012) 1657–1677, https://doi.org/10.1016/j.progpolymsci.2012.07.005.

[4] P. Müller, B. Imre, J. Bere, J. Móczó, B. Pukánszky, Physical ageing and molecular mobility in PLA blends and composites, J. Therm. Anal. Calorim. 122 (2015) 1423–1433, https://doi.org/10.1007/s10973-015-4831-6.

[5] R. Auras, B. Harte, S. Selke, An overview of polylactides as packaging materials, Macromol. Biosci. 4 (2004) 835–864, https://doi.org/10.1002/mabi.200400043.

[6] D. Maillard, R.E. Prud, Homme, crystallization of ultrathin films of polylactides: from chain chirality to lamella curvature and twisting, Macromolecules 41 (2008) 1705–1712, https://doi.org/10.1021/ma071306u.

[7] H. Bai, W. Zhang, H. Deng, Q. Zhang, Q. Fu, Control of crystal morphology in poly (l-lactide) by adding nucleating agent, Macromolecules 44 (2011) 1233–1237, https://doi.org/10.1021/ma102439t.

[8] Z. Gui, C. Lu, S. Cheng, Comparison of the effects of commercial nucleation agents on the crystallization and melting behaviour of polylactide, Polym. Test. 32 (2013) 15–21, https://doi.org/10.1016/j.polymertesting.2012.08.011.

[9] L. Jiang, T. Shen, P. Xu, X. Zhao, X. Li, W. Dong, P. Ma, M. Chen, Crystallization modification of poly(lactide) by using nucleating agents and stereocomplexation, E-Polymers 16 (2016) 1–13, https://doi.org/10.1515/epoly-2015-0179.

[10] C. Sun, C. Li, H. Tan, Y. Zhang, Enhancing the durability of poly(lactic acid) composites by nucleated modification, Polym. Int. 68 (2019) 1450–1459, https://doi.org/10.1002/pi.5837.

[11] A.M. Harris, E.C. Lee, Improving mechanical performance of injection molded PLA by controlling crystallinity, J. Appl. Polym. Sci. 107 (2008) 2246–2255, https://doi.org/10.1002/app.27261.

[12] A. Kovalcik, R.A. Pérez-Camargo, C. Fürst, P. Kucharczyk, A.J. Müller, Nucleating efficiency and thermal stability of industrial non-purified lignins and ultrafine talc in poly(lactic acid) (PLA), Polym. Degrad. Stabil. 142 (2017) 244–254, https://doi.org/10.1016/j.polymdegradstab.2017.07.009.

[13] J.Y. Nam, S. Sinha Ray, M. Okamoto, Crystallization behavior and morphology of biodegradable polylactide/layered silicate nanocomposite, Macromolecules 36 (2003) 7126–7131, https://doi.org/10.1021/ma034623j.

[14] S. Barrau, C. Vanmansart, M. Moreau, A. Addad, G. Stoclet, J.M. Lefebvre, R. Seguela, Crystallization behavior of carbon Nanotube−Polylactide nanocomposites, Macromolecules 44 (2011) 6496–6502, https://doi.org/10.1021/ma200842n.

[15] H. Wang, Z. Qiu, Crystallization kinetics and morphology of biodegradable poly(L-lactic acid)/graphene oxide nanocomposites: influences of graphene oxide loading and crystallization temperature, Thermochim. Acta (2012) 40–46, https://doi.org/10.1016/jtca201110004.

[16] K. Pongtanayut, C. Thongpin, O. Santawitee, The effect of rubber on morphology, thermal properties and mechanical properties of PLA/NR and PLA/ENR blends, Energy Proc. 34 (2013) 888–897, https://doi.org/10.1016/j.egypro.2013.06.826.

[17] I. Fekete, F. Ronkay, L. Lendvai, Highly toughened blends of poly(lactic acid) (PLA) and natural rubber (NR) for FDM-based 3D printing applications: the effect of composition and infill pattern, Polym. Test. 99 (2021) 107205, https://doi.org/10.1016/j.polymertesting.2021.107205.

[18] Y. Huang, M.T. Müller, R. Boldt, C. Zschech, U. Gohs, S. Wießner, A new strategy to improve viscoelasticity, crystallization and mechanical properties of polylactide, Polym. Test. 97 (2021) 107160, https://doi.org/10.1016/j.polymertesting.2021.107160.

[19] A. Kowalewska, M. Nowacka, Supramolecular interactions in hybrid polylactide blends—the structures, mechanisms and properties, Molecules 25 (2020), https://doi.org/10.3390/molecules25153351.

[20] S. Liu, Y. He, J.-P. Qu, Manufacturing high-performance polylactide by constructing 3D network crystalline structure with adding self-assembly nucleator, Ind. Eng. Chem. Res. 61 (2022) 4567–4578, https://doi.org/10.1021/acs.iecr.2c00133.

[21] W. Wang, A. Saperdi, A. Dodero, M. Castellano, A.J. Müller, X. Dong, D. Wang, D. Cavallo, Crystallization of a self-assembling nucleator in poly(l-lactide) melt, Cryst. Growth Des. 21 (2021) 5880–5888, https://doi.org/10.1021/acs.cgd.1c00750.

[22] H. Nakajima, M. Takahashi, Y. Kimura, Induced crystallization of PLLA in the presence of 1,3,5-benzenetricarboxylamide derivatives as nucleators: preparation of haze-free crystalline PLLA materials, Macromol. Mater. Eng. 295 (2010) 460–468, https://doi.org/10.1002/mame.200900353.

[23] H. Bai, C. Huang, H. Xiu, Q. Zhang, H. Deng, K. Wang, F. Chen, Q. Fu, Significantly improving oxygen barrier properties of polylactide via constructing parallel-aligned shish-kebab-like crystals with well-interlocked boundaries, Biomacromolecules 15 (2014) 1507–1514, https://doi.org/10.1021/bm500167u.

[24] Q. Xing, R. Li, X. Zhang, X. Dong, D. Wang, L. Zhang, Tailoring crystallization behavior of poly (l-lactide) with a low molecular weight aliphatic amide, Colloid Polym. Sci. 293 (2015) 3573–3583, https://doi.org/10.1007/s00396-015-3730-5.

[25] N. Kawamoto, A. Sakai, T. Horikoshi, T. Urushihara, E. Tobita, Nucleating agent for poly(L-lactic acid)—an optimization of chemical structure of hydrazide compound for advanced nucleation ability, J. Appl. Polym. Sci. 103 (2007) 198–203, https://doi.org/10.1002/app.25109.

[26] H. Zhang, H. Bai, Z. Liu, Q. Zhang, Q. Fu, Toward high-performance poly(l-lactide) fibers via tailoring crystallization with the aid of fibrillar nucleating agent, ACS Sustain. Chem. Eng. 4 (2016) 3939–3947, https://doi.org/10.1021/acssuschemeng.6b00784.

[27] Z. Qiu, Z. Li, Effect of orotic acid on the crystallization kinetics and morphology of biodegradable poly(l-lactide) as an efficient nucleating agent, Ind. Eng. Chem. Res. 50 (2011) 12299–12303, https://doi.org/10.1021/ie2019596.

[28] N. Petchwattana, P. Naknaen, J. Sanetuntikul, B. Narupai, Crystallisation behaviour and transparency of poly(lactic acid) nucleated with dimethylbenzylidene sorbitol, Plastics, Rubber and Composites 47 (2018) 147–155, https://doi.org/10.1080/14658011.2018.1447338.

[29] B.O. Okesola, V.M.P. Vieira, D.J. Cornwell, N.K. Whitelaw, D.K. Smith, 1,3:2,4-Dibenzylidene-d-sorbitol (DBS) and its derivatives – efficient, versatile and industrially-relevant low-molecular-weight gelators with over 100 years of history and a bright future, Soft Matter 11 (2015) 4768–4787, https://doi.org/10.1039/C5SM00845J.

[30] C.R. Xie, R. Lee, Todd D. Danielson, Dibenzylidene Sorbitol (DBS)-Based Compounds, Compositions and Methods for Using Such Compounds, 2007.

[31] W.-C. Lai, Y.-C. Lee, Effects of self-assembled sorbitol-derived compounds on the structures and properties of biodegradable poly(L-lactic acid) prepared by melt blending, J. Polym. Res. 26 (2018) 10, https://doi.org/10.1007/s10965-018-1670-8.

[32] K. Bernland, T. Tervoort, P. Smith, Phase behavior and optical- and mechanical properties of the binary system isotactic polypropylene and the nucleating/clarifying agent 1,2,3-trideoxy-4,6:5,7-bis-O-[(4-propylphenyl) methylene]-nonitol, Polymer 50 (2009) 2460–2464, https://doi.org/10.1016/j.polymer.2009.03.010.

[33] E.W. Fischer, H.J. Sterzel, G. Wegner, Investigation of the structure of solution grown crystals of lactide copolymers by means of chemical reactions, Kolloid-Z. Z. Polym. 251 (1973) 980–990, https://doi.org/10.1007/BF01498927.

[34] Z. Horváth, B. Gyarmati, A. Menyhárd, P. Doshev, M. Gahleitner, J. Varga, B. Pukánszky, The role of solubility and critical temperatures for the efficiency of sorbitol clarifiers in polypropylene, RSC Adv. 4 (2014) 19737–19745, https://doi.org/10.1039/C4RA01917B.

[35] Z. Horváth, A. Menyhárd, P. Doshev, M. Gahleitner, G. Vörös, J. Varga, B. Pukánszky, Effect of the molecular structure of the polymer and nucleation on

the optical properties of polypropylene homo- and copolymers, ACS Appl. Mater. Interfaces 6 (2014) 7456–7463, https://doi.org/10.1021/am5008535.
[36] A. Menyhárd, M. Gahleitner, J. Varga, K. Bernreitner, P. Jääskeläinen, H. Øysæd, B. Pukánszky, The influence of nucleus density on optical properties in nucleated isotactic polypropylene, Eur. Polym. J. 45 (2009) 3138–3148, https://doi.org/10.1016/j.eurpolymj.2009.08.006.
[37] K. Wasanasuk, K. Tashiro, Crystal structure and disorder in Poly(l-lactic acid) δ form (α′ form) and the phase transition mechanism to the ordered α form, Polymer 52 (2011) 6097–6109, https://doi.org/10.1016/j.polymer.2011.10.046.
[38] E. Suljovrujic, D. Milicevic, On the enthalpy of melting of poly(l-lactide), Int. J. Polym. Anal. Char. 24 (2019) 381–388, https://doi.org/10.1080/1023666X.2019.1598635.
[39] W.-C. Lai, Thermal behavior and crystal structure of poly(l-lactic acid) with 1,3:2,4-Dibenzylidene-d-sorbitol, J. Phys. Chem. B 115 (2011) 11029–11037, https://doi.org/10.1021/jp2037312.
[40] P. Pan, B. Zhu, W. Kai, T. Dong, Y. Inoue, Effect of crystallization temperature on crystal modifications and crystallization kinetics of poly(L-lactide), J. Appl. Polym. Sci. 107 (2008) 54–62, https://doi.org/10.1002/app.27102.
[41] P. Pan, B. Zhu, W. Kai, T. Dong, Y. Inoue, Polymorphic transition in disordered poly (l-lactide) crystals induced by annealing at elevated temperatures, Macromolecules 41 (2008) 4296–4304. https://10.1021/ma800343g.
[42] P.E. Le Marec, L. Ferry, J.-C. Quantin, J.-C. Bénézet, F. Bonfils, S. Guilbert, A. Bergeret, Influence of melt processing conditions on poly(lactic acid) degradation: molar mass distribution and crystallization, Polym. Degrad. Stabil. 110 (2014) 353–363, https://doi.org/10.1016/j.polymdegradstab.2014.10.003.
[43] S.C. Schmidt, M.A. Hillmyer, Polylactide stereocomplex crystallites as nucleating agents for isotactic polylactide, J. Polym. Sci. B Polym. Phys. 39 (2001) 300–313, https://doi.org/10.1002/1099-0488(20010201)39:3<300::AID-POLB1002>3.0.CO;2.
[44] J. Narita, M. Katagiri, H. Tsuji, Highly enhanced nucleating effect of melt-recrystallized stereocomplex crystallites on poly(L-lactic acid) crystallization, Macromol. Mater. Eng. 296 (2011) 887–893, https://doi.org/10.1002/mame.201100024.
[45] N. Rahman, T. Kawai, G. Matsuba, K. Nishida, T. Kanaya, H. Watanabe, H. Okamoto, M. Kato, A. Usuki, M. Matsuda, K. Nakajima, N. Honma, Effect of polylactide stereocomplex on the crystallization behavior of poly(l-lactic acid), Macromolecules 42 (2009) 4739–4745, https://doi.org/10.1021/ma900004d.
[46] S. Saeidlou, M.A. Huneault, H. Li, P. Sammut, C.B. Park, Evidence of a dual network/spherulitic crystalline morphology in PLA stereocomplexes, Polymer 53 (2012) 5816–5824, https://doi.org/10.1016/j.polymer.2012.10.030.
[47] W.-C. Lai, The effect of self-assembled nanofibrils on the morphology and microstructure of poly(l-lactic acid), Soft Matter 7 (2011) 3844–3851, https://doi.org/10.1039/C0SM01170C.
[48] M.L. Di Lorenzo, R. Androsch, Influence of α′-/α-crystal polymorphism on properties of poly(l-lactic acid), Polym. Int. 68 (2019) 320–334, https://doi.org/10.1002/pi.5707.
[49] M. Avrami, Kinetics of phase change. I general theory, J. Chem. Phys. 7 (1939) 1103–1112, https://doi.org/10.1063/1.1750380.
[50] H. Tsuji, H. Takai, S.K. Saha, Isothermal and non-isothermal crystallization behavior of poly(l-lactic acid): effects of stereocomplex as nucleating agent, Polymer 47 (2006) 3826–3837, https://doi.org/10.1016/j.polymer.2006.03.074.
[51] L. Mandelkern, Crystallization of Polymers: Volume 1: Equilibrium Concepts, 2 ed., Cambridge University Press, Cambridge, 2002.
[52] A.T. Lorenzo, M.L. Arnal, J. Albuerne, A.J. Müller, DSC isothermal polymer crystallization kinetics measurements and the use of the Avrami equation to fit the data: guidelines to avoid common problems, Polym. Test. 26 (2007) 222–231, https://doi.org/10.1016/j.polymertesting.2006.10.005.
[53] K. Bernland, J.G.P. Goossens, P. Smith, T.A. Tervoort, On clarification of haze in polypropylene, J. Polym. Sci. B Polym. Phys. 54 (2016) 865–874, https://doi.org/10.1002/polb.23992.
[54] J. Li, K. Fan, X. Guan, Y. Yu, J. Song, Self-assembly mechanism of 1,3:2,4-Di(3,4-dichlorobenzylidene)-d-sorbitol and control of the supramolecular chirality, Langmuir 30 (2014) 13422–13429, https://doi.org/10.1021/la5034178.